Theoretical Study of the $C_2(^1\Sigma_g^+,^3\Pi_u) + H_2O$ Reaction Mechanism

Jia-Hai Wang,[†] Ke-Li Han,*[,†] Guo-Zhong He,[†] Zhuangjie Li,*[,†,‡,||] and Vernon R. Morris[§]

State Key Laboratory of Molecular Reaction Dynamics, Dalian Institute of Chemical Physics, Chinese Academy of Sciences, Dalian 116023, China, Department of Atmospheric Sciences, University of Illinois at Urbana-Champaign, Urbana, Illinois 61801, and Department of Chemistry, Howard University, Washington, D.C. 20059

Received: March 7, 2003; In Final Form: July 14, 2003

The reaction of C_2 with water and the possible subsequent reactions have been investigated using ab initio methods. Species involved in the reactions on both singlet and triplet potential energy surfaces were optimized at both Møller−Plesset correlation energy correction truncated at second-order (MP2) and quadratic configuration interaction including single and double substitution (QCISD) levels in conjunction with the 6-311++G** basis set. Single point calculations were performed using coupled cluster theory including single, double, and triple substitutions (CCSD(T)) in conjunction with the 6-311++G(d,pd) basis set with the geometry optimized at the MP2/6-311++G** level. On the basis of computational energetic results at the CCSD(T)/6-311++G(d,pd)//MP2/6-311++G** plus zero point energy correction level of theory the association reaction channel on the singlet surface dominates over the H-abstraction channel on both singlet and triplet surfaces. The most feasible reaction following the formation of association intermediate ($CCOH_2$) is the intramolecular hydrogen migration leading to hydroxyethyne (HCCOH). Rearrangement of HCCOH can lead to several other isomer intermediates. Elimination of atomic and molecular hydrogen from HCCOH, $CCOH_2$, and other isomer intermediates is also surveyed. The implication of our computational results regarding the reaction of C_2 with H_2O in interstellar space and combustion process is discussed.

1. Introduction

Chemical processes involving C_2 have been of great significance in the study of both high-temperature chemistry and astrophysical sciences.[1−5] Investigation of the C_2 related reactions has invoked great inclination due to their important role in exploring high-temperature chemistry of hydrocarbons. C_2 has been involved in soot formation in hot flames, in diamond synthesis from gas pyrolysis, and in the formation and decay of the newly discovered C_{60} fullerenes.[2−4] In astrophysical science C_2 has been detected in the atmospheric carbon stars, comets, and diffuse and translucent clouds.[1,5] Investigation of chemistry involving C_2 has been of astrophysical interest in the studies of a variety of interstellar objects.[1,5] The reactions of C_2 with C_2H_2, C_2H_4, N_2, H_2, and H_2S have been investigated in detail either experimentally or theoretically,[6−11] but to the best of our knowledge, there is very little information available regarding the detailed mechanism for the reaction of C_2 with H_2O,

$$C_2 + H_2O \rightarrow \text{products} \qquad (1)$$

This reaction cannot be neglected in molecular clouds[12−14] and circumstellar space because recent observations with submillimeter wave astronomy satellite indicated that there is gaseous H_2O in clumpy molecular clouds.[15] Spectroscopic results from ISO (IR Space Observatory, Kessler et al., 1996) revealed a wealth of interesting features and particular absorption signatures of solid-state interstellar ice H_2O.[16] Understanding the mechanism of reaction 1 will give access to interstellar complex activities, so the investigation of interaction between C_2 and water molecules is called for to model the interstellar composition. Though it is difficult to experimentally observe and characterize all possible intermediate species involved in reaction 1, the ab initio method is a useful tool to provide insight for such a complex reaction system. In this paper we report our ab initio study for reaction 1. The present work aims at characterizing the reaction pathways on both triplet and singlet potential energy surfaces. We also explore several additional reactions following the association of a water molecule to C_2, define possible intermediates and products associated with these reactions, and examine the energetics of these processes.

2. Theoretical Approaches

All calculations were implemented using the Gaussian-98 program.[17] Preliminary structural optimization of reactants, products, and transition states for reaction 1 and subsequent processes was carried out with Møller−Plesset correlation energy correction truncated at the second-order level (MP2)[18−24] in conjunction with the 6-311++G**[25] basis set. The initial calculation results were checked for consistency by carrying out calculations using the quadratic configuration[26] interaction including single and double substitutions (QCISD)[27] in most cases. To obtain a better accuracy for species with very small force constants, such as $CCOH_2$, we employ a tight option for convergence. Frequency calculations were computed by determining force constants analytically at the MP2/6-311++G** level of theory for most of the species, and numerically at the

* To whom correspondence should be addressed. E-mail: klhan@dicp.ac.cn, zli@atmos.uiuc.edu.
† Chinese Academy of Sciences.
‡ University of Illinois at Urbana-Champaign.
§ Howard University.
|| Current address: Department of Chemistry and Biochemistry, California State University Fullerton, Fullerton, CA 92834-6808. E-mail: zli@exchange.fullerton.edu.

10.1021/jp0345912 CCC: $25.00
Published on Web 10/23/2003

TABLE 1: Relative Energy (kcal mol^{-1}) Referenced to $CC(^1\Sigma_g^+) + H_2O(X^1A_1)$ for Complex and Intermediate Isomers

species	ΔE(MP2[a]+ZPE)	ΔE(CCSD(T)[b]+ ZPE)	ZPE
PRT2	−1.3	−1.8	17.9
I1	−7.5	−6.4	19.7
I2	−112.9	−107.4	19.7
I3	−81.7	−81.0	20.5
I4	−147.3	−140.9	19.7
I5	−67.6	−63.7	18.1
I6[c]	−57.3	−59.7	19.3

[a] Calculation in conjunction with the 6-311++G** basis set,** mean polarization functions. [b] Single point calculation in conjunction with the 6-311G++(d,dp) basis set using geometry optimized at the MP2/6-311++G** level of theory. [c] Geometry optimized at the QCISD/6-311++G** level of theory.

TABLE 2: Relative Energy (kcal mol^{-1}) Referenced to $CC(^1\Sigma_g^+) + H_2O(X^1A_1)$ for Reactants and Other Species

species	ΔE(MP2[a]+ZPE)	ΔE(CCSD(T)[b]+ZPE)	ZPE
$CC(^1\Sigma_g^+) + H_2O$	0.0	0.0	16.3
$CC(^3\Pi_u) + H_2O$	5.0	1.5	16.0
CCH + OH	10.3	14.0	16.5
CCOH + H	12.2	15.8	12.4
$CCO + H_2$	−22.9	−21.8	12.0
c-COC + H_2	−9.3	−7.4	11.0
c-HCOC + H	8.4	15.8	13.0
HCCO + H	−47.0	−36.4	12.5
$H_2C + CO$	−58.8	−61.7	13.7

[a] Calculation in conjunction with 6-311++G** basis set. [b] Single point calculation in conjunction with the 6-311++G(d,pd) basis set using geometry optimized at the MP2/6-311++G** level of theory.

QCISD/6-311++G** level of theory for CCHOH and the transition state complex associated with CCHOH. In the case of ambiguous imaginary vibration motions, we simultaneously used the displacement vector and dipole derivative unit vector to verify the expected transition states. The intrinsic reaction coordinate (IRC)[28,29] calculation was performed to check whether the optimized transition state connected to proper reactants and products. Finally, the single point energy was calculated using the coupled cluster correlation method including single, double, and triple substitutions (CCSD(T))[30,31] in conjunction with the 6-311++G(d,pd) basis set (CCSD(T)/6-311++G(d,pd)) utilizing the geometry optimized at the MP2/6-311++G** level of theory. The best estimate of energetics was then determined by adding zero point energy correction to the results calculated at the CCSD(T)/6-311++G(d,pd)//MP2/6-311++G** level of theory.

3. Results and Discussion

Optimized structural parameters for reactants, products, and transition state complex species involved in reaction 1 and subsequent reactions are provided in Figure 1. The total energy for each of the species is given in Tables 1−3. The energy level of each chemical process relative to that of the $CC(^1\Sigma_g^+) + H_2O(X^1A_1)$ reactants is also given in Tables 1−3 and summarized in Figure 2. The calculated vibration frequency for the key species is listed in Table 4. Moments of inertia are provided in the Supporting Information. The optimized reactant and product species are found to each have all positive frequencies, indicating that the species is a local minimum on the potential energy surface. The optimized transition state configuration for each chemical process possesses an imaginary frequency, indicating a saddle point on the potential surface for the located transition state configuration.

TABLE 3: Relative Energy (kcal mol^{-1}) Referenced to $CC(^1\Sigma_g^+) + H_2O(X^1A_1)$ for Transition State Complex Species

species	ΔE(MP2[a]+ZPE)	ΔE(CCSD(T)[b]+ZPE)	ZPE
T1	10.6	13.8	16.0
3T1	34.6	41.4	14.9
T2	5.1	−1.0	19.1
T3	6.0	6.5	16.3
T3a	41.2	31.2	12.7
T3b	51.9[e]	19.0	12.8
T3c	−54.3	−46.9	15.7
T3d1	−9.8	−12.5	15.8
T3d2	11.2	10.9	13.4
T3d3[d]	48.9[e]	26.9	10.1
T3e1[c]		−59.7	17.2
T4	−27.9	−26.1	16.9
T5	60.0	−61.3	17.7
T6a	−34.1	−26.8	16.4
T6c	−28.0	−31.8	18.2
T6d[c]		-61.6	17.8
T8a	56.0	−58.7	16.4

[a] Calculation in conjunction with 6-311++G** basis set. [b] Single point calculation in conjunction with 6-311++G(d,dp) basis set using geometry optimized at MP2/6-311++G** level of theory. [c] Structure optimized at the QCISD/6-311++G** level of theory. For T6d see text discussion. For T3e1, this is preferred due to there being large spin contamination involved in the MP2/6-311++G** optimization, leading to a very different structure. [d] H2 energy is added to the energy of the transition state so that the total energy of T3d3 can be comparable with that of the reactants. [e] The relative energies are significantly different from the results of the CCSD(T)/6-311++G(d,pd)//MP2/6-311++G**level. The reason we still choose the structure based on MP2/6-311++G** is provided in the main text.

One important pathway for the reaction of C_2 with H_2O is the association reaction to form an intermediate, $CCOH_2$. Other possible reaction channels include the H-abstraction from H_2O either on a triplet or on a singlet potential energy surface, leading to the formation of CCH and OH radicals. Therefore, the following discussion has been concentrated on the association reaction leading to the formation of $CCOH_2$ (signified as **I1**) and the H-abstraction reactions. We will also explore the subsequent reactions following the formation of **I1** and H-abstraction reactions, which result in final products of the reaction 1. For convenience we have designated the stationary intermediates species and products, which is characterized with positive frequency for all vibrational modes, by **I** appended by a number (1, 2, and so on), respectively, e.g., **I1**, **I2**, ..., etc. Similarly, the transition state intermediate complex is designated either by T appended by number or by a combination of T with small letters, e.g., T1, T2, T3, T3a, T3b, T3c1 etc.

3.1. H-Abstraction from $H_2O(X^1A_1)$ by $CC(^1\Sigma_g^+)$ and $CC(^3\Pi_u)$. The optimized structure of the transition state complex for H-abstraction reaction on both singlet and triplet potential energy sufaces,

$$CC(^1\Sigma_g^+) + H_2O(X^1A_1) \rightarrow [CC\cdots H\cdots OH\ (T1)]^{\ddagger} \rightarrow CCH(^2\Sigma^+) + OH(^2\Sigma^+) \quad (1a)$$

$$CC(^3\Pi_u) + H_2O(X^1A_1) \rightarrow [CC\cdots H\cdots OH\ (3T1)]^{\ddagger} \rightarrow CCH(^2\Sigma^+) + OH(^2\Sigma^+) \quad (1b)$$

is shown in Figure 1 as T1 and 3T1, respectively. These structures were located at the MP2/6-311++G** level of theory. Our calculation results indicate that the C2−H1 bond in the transition state is shorter by ca. 0.06 Å on the singlet surface than on the triplet surface, but the O−H1 bond is longer by ca. 0.06 Å, and the C1−C2 bond is longer by 0.05 Å, respectively. The C2−H1 bond and O−H1 bond is predicted to be collinear

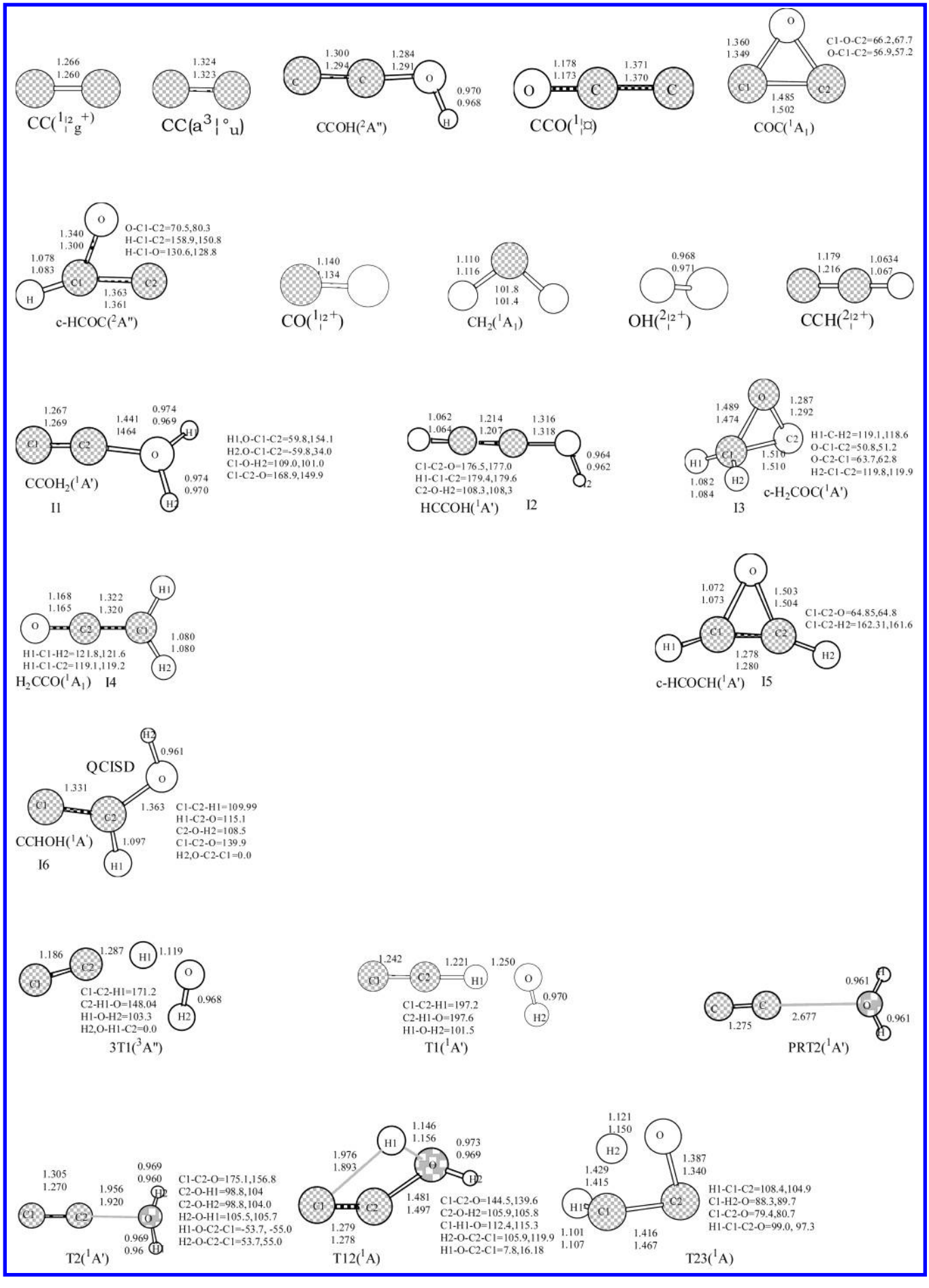
1.266
1.260
CC(1Σg+)
1.324
1.323
CC(a3Πu)
1.300
1.294
1.284
1.291
0.970
0.968
CCOH(2A")
1.178
1.173
1.371
1.370
CCO(1Σ)
1.360
1.349
1.485
1.502
C1-O-C2=66.2,67.7
O-C1-C2=56.9,57.2
COC(1A1)
1.340
1.300
1.078
1.083
1.363
1.361
O-C1-C2=70.5,80.3
H-C1-C2=158.9,150.8
H-C1-O=130.6,128.8
c-HCOC(2A")
1.140
1.134
CO(1Σ+)
1.110
1.116
101.8
101.4
CH2(1A1)
0.968
0.971
OH(2Σ+)
1.179
1.216
1.0634
1.067
CCH(2Σ+)
1.267
1.269
1.441
1464
0.974
0.969
0.974
0.970
H1,O-C1-C2=59.8,154.1
H2,O-C1-C2=-59.8,34.0
C1-O-H2=109.0,101.0
C1-C2-O=168.9,149.9
CCOH2(1A')
I1
1.062
1.064
1.214
1.207
1.316
1.318
0.964
0.962
C1-C2-O=176.5,177.0
H1-C1-C2=179.4,179.6
C2-O-H2=108.3,108,3
HCCOH(1A')
I2
1.489
1.474
1.287
1.292
1.510
1.510
1.082
1.084
H1-C-H2=119.1,118.6
O-C1-C2=50.8,51.2
O-C2-C1=63.7,62.8
H2-C1-C2=119.8,119.9
c-H2COC(1A')
I3
1.168
1.165
1.322
1.320
1.080
1.080
H1-C1-H2=121.8,121.6
H1-C1-C2=119.1,119.2
H2CCO(1A1)
I4
1.072
1.073
1.503
1.504
1.278
1.280
C1-C2-O=64.85,64.8
C1-C2-H2=162.31,161.6
c-HCOCH(1A')
I5
QCISD
0.961
1.331
1.363
1.097
C1-C2-H1=109.99
H1-C2-O=115.1
C2-O-H2=108.5
C1-C2-O=139.9
H2,O-C2-C1=0.0
CCHOH(1A')
I6
1.186
1.287
1.119
0.968
C1-C2-H1=171.2
C2-H1-O=148.04
H1-O-H2=103.3
H2,O-H1-C2=0.0
3T1(3A")
1.242
1.221
1.250
0.970
C1-C2-H1=197.2
C2-H1-O=197.6
H1-O-H2=101.5
T1(1A')
0.961
2.677
0.961
1.275
PRT2(1A')
1.305
1.270
0.969
0.960
1.956
1.920
0.969
0.96
C1-C2-O=175.1,156.8
C2-O-H1=98.8,104
C2-O-H2=98.8,104.0
H2-O-H1=105.5,105.7
H1-O-C2-C1=-53.7, -55.0
H2-O-C2-C1=53.7,55.0
T2(1A')
1.146
1.156
1.976
1.893
0.973
0.969
1.481
1.497
1.279
1.278
C1-C2-O=144.5,139.6
C2-O-H2=105.9,105.8
C1-H1-O=112.4,115.3
H2-O-C2-C1=105.9,119.9
H1-O-C2-C1=7.8,16.18
T12(1A)
1.121
1.150
1.429
1.415
1.387
1.340
1.101
1.107
1.416
1.467
H1-C1-C2=108.4,104.9
C1-H2-O=88.3,89.7
C1-C2-O=79.4,80.7
H1-C1-C2-O=99.0, 97.3
T23(1A)

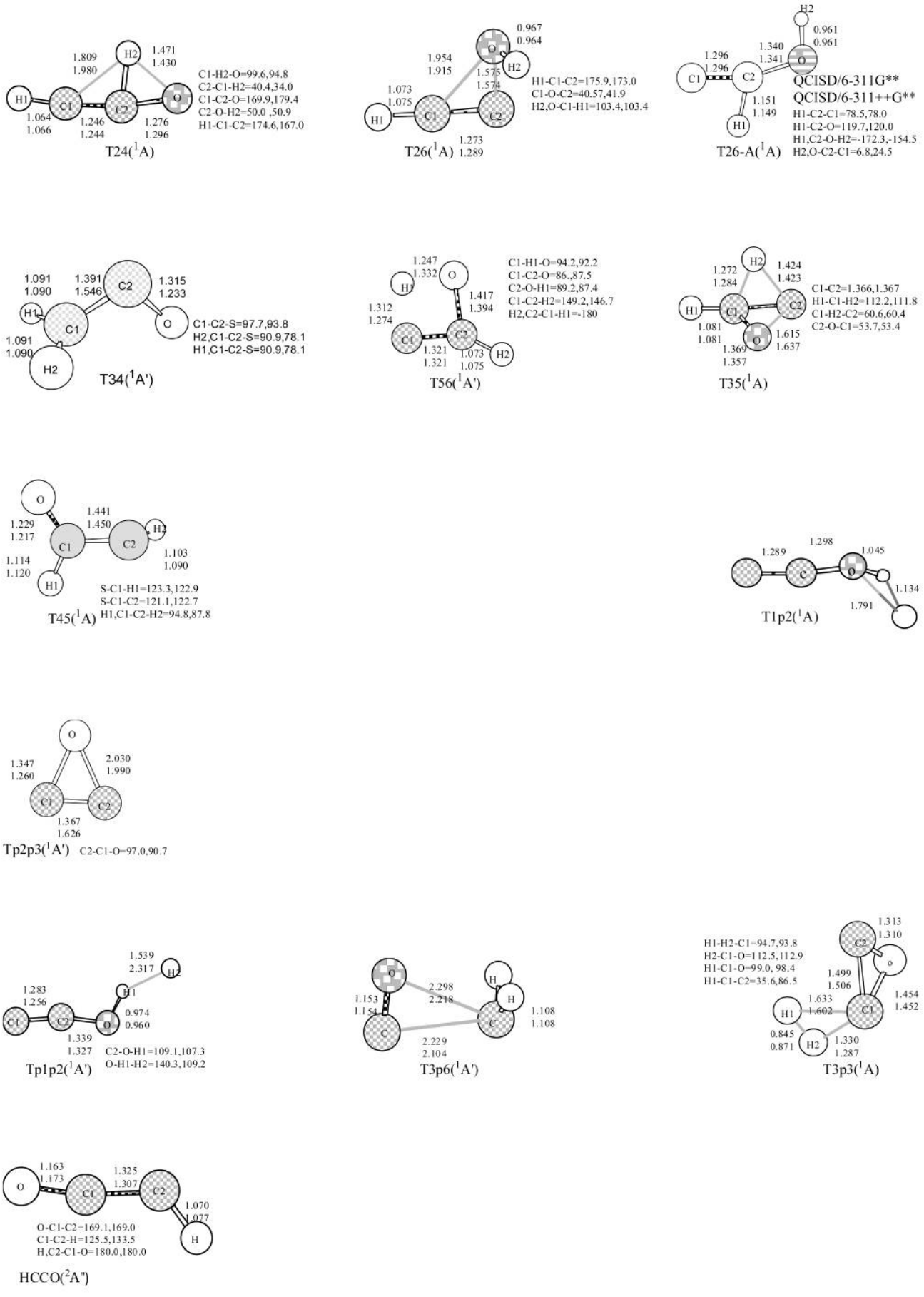

Figure 1. Structural parameters optimized at MP2 (top or first values) and QCISD (bottom or second values) levels of theory in conjunction with 6-311++G** basis set.

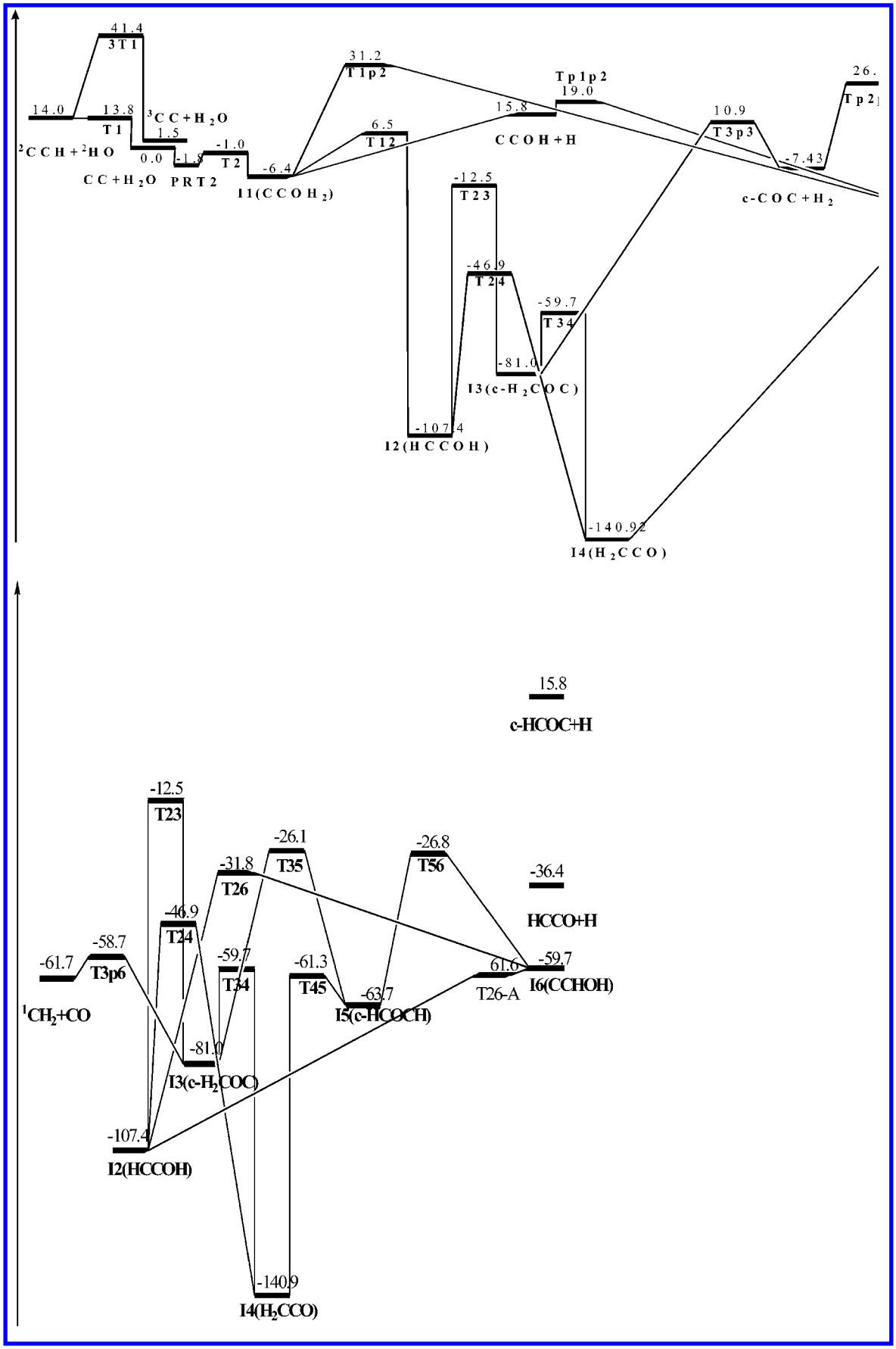

Figure 2. (a) Schematic illustration of energy (kcal·mol^{-1}) relative to $CC(^1\Sigma_g^+)$ + $H_2O(X^1A_1)$. The values are computed at CCSD(T)/6-311++G(d,pd)//MP2/6-311++G** + ZPE level of theory. (b) Schematic illustration of energy (kcal·mol^{-1}) relative to $CC(^1\Sigma_g^+)$ + $H_2O(X^1A_1)$. The values are computed at CCSD(T)/6-311++G(d,pd)//MP2/6-311++G** + ZPE level of theory.

TABLE 4: Vibration Frequencies (cm^{-1}) Calculated at the MP2/6-311++G Level of Theory for Reactants, Small Species, and Transition State Complex Species Involved in $C_2 + H_2O$ and Subsequent Reactions[a]**

species	frequency
$CCOH_2$	54, 119, 718, 854, 1028, 1615, 1928, 3675, 3773
HCCOH	351, 360, 543, 614, 1074, 1264, 2223, 3526, 3859
c-H_2COC	816, 858, 902, 1115, 1139, 1438, 1553, 3189, 3314
H_2CCO	423, 437, 571, 987, 1153, 1412, 2219, 3231, 3343
c-HCOCH	32, 517, 593, 891, 962, 1089, 1764, 3371, 3441
CCHOH	(273, 313, 716, 999, 1117, 1374, 1712, 3122, 3886)
CCOH	262, 315, 1061, 1261, 2032, 3762
HCCO	526, 596, 669, 1237, 2375, 3322
c-HCOC	769, 961, 1057, 1358, 1570, 3343
CCO	332, 458, 1084, 2000
c-CCO	929, 943, 1405
CCH	831, 831, 2461, 3572
PRT2	110, 119, 168, 404, 452, 1626, 1809, 3860, 3981 3859.8, 3980.6.
T1	2088i, 156, 159, 637, 732, 1599, 1940, 2183, 3786
3T1	2801i, 146, 197, 490, 551, 926, 1574, 2688, 3837
T2	393i, 390, 402, 807, 901, 1600, 1605, 3753, 3882
T3	1584i, 201, 238, 778, 1099, 1114, 1830, 2428, 3733
T3a	1693i, 246, 308, 666, 892, 1056, 1174, 2042, 2529
T3b	986i, 197, 304, 387, 795, 946, 1019, 1946, 3347
T3c	1522i, 75, 236, 533, 535, 1216, 2137, 2748, 3509
T3d1	1509i, 578, 784, 930, 962, 1115, 1324, 2287, 3103
T3d2	1014i, 488, 575, 800, 836, 986, 1370, 1480, 3042
T3d3	1192i, 1156, 1415
T3e1	(1363i, 194, 679, 857, 946, 1410, 1554, 3125, 3262)
T4	1153i, 522, 942, 1060, 1214, 1229, 1515, 2059, 3293
T5	241i, 542, 722, 982, 1079, 1393, 1652, 2908, 3091
T6a	1670i, 558, 710, 816, 961, 1120, 1609, 2287, 3395
T6c	734i, 447, 498, 735, 966, 1157, 1697, 3422, 3819
T6d	(361i, 203, 476, 846, 1058, 1339, 1911, 2745, 3893)
T8a	217i, 179, 243, 684, 859, 1391, 2014, 3015, 3114

[a] The values in parentheses are calculated at the QCISD/6-311++G** level of theory.

on the singlet potential surface, but to form an angle of 148.0° on the triplet surface.

Energetically, our calculation at the CCSD(T)/6-311++G(d,pd)//MP2/6-311++G** + ZPE level of theory predicts a triplet−singlet state separation energy of 1.5 kcal mol^{-1} for the C_2 molecule, which is in good agreement with the experimental value of 2.0 kcal mol^{-1}.[32] The bond lengths of singlet C_2 and triplet C_2 are 1.260 and 1.323 Å, respectively, based on QCISD/6-311++G**, which is similar to 1.266 and 1.324 Å based on MP2/6-311++G**. This indicates that it is appropriate to employ the results computed at the CCSD(T)/6-311++G(d,pd)//MP2/6-311++G** + ZPE level of theory to provide data with an uncertainty of ±1 kcal mol^{-1} for illustrating the reaction mechanisms in the present study. An activation energy of 13.8 and 41.4 kcal mol^{-1} is predicted for the H-abstraction by C_2 on the singlet and triplet potential energy surface, respectively. Because the heat of reaction on the singlet surface is computed to be 14.0 kcal mol^{-1}, which is greater than the calculated activation energy (13.8 kcal mol^{-1}), the reverse reaction of H-abstraction on the singlet potential surface may be a barrierless process. The large barrier on the triplet potential surface is so unconceivable, but IRC definitely points to the above reactants and products. The triplet transition state cannot be located by B3LYP and QCISD. What merits our mention is that another triplet C_2 structure has been located by QCISD/6-311++G** and MP2/6-311++G**, and the bond length is also shorter than the singlet bond length.

Recombination of the CCH and OH produced from the H-abstraction reactions 1a and 1b may lead to the formation of HCCOH (**I2**),

$$CCH(^2\Sigma^+) + OH(^2\Sigma^+) \rightarrow HCCOH \quad (2)$$

with an exothermicity of 121.4 kcal mo1^{-1} on the basis of our calculation at the CCSD(T)/6-311G(d,pd)//MP2/6-311++G** + ZPE level of theory.

3.2. Association Reaction and Subsequent Reactions. The association reaction pathway of $CC(^1\Sigma_g^+) + H_2O(X^1A_1)$ results in the formation of $CCOH_2$ (**I1**). Further investigation of this reaction channel suggests that the association proceeds by first forming a van der Waals complex precomplex (**PRT2**), which is featured by a long C2−O bond (2.677 Å), as shown in Figure 1. The **PRT2** is 1.8 kcal mol^{-1} below the $CC(^1\Sigma_g^+) + H_2O(X^1A_1)$ reactants. Shortening the C2−O bond in **PRT2** by ca. 1.2 Å leads to the formation of **I1** through a transition state (**T2**) with a C2−O bond length of 1.956 Å (see Figure 1),

$$CC(^1\Sigma_g^+) + H_2O(X^1A_1) \rightarrow \mathbf{PRT2} \rightarrow [CC\cdots OH_2\ (T2)]^{\ddagger} \rightarrow CCOH_2 \quad (1c)$$

A low activation energy of 0.8 kcal mol^{-1} is expected on the basis of our calculation at the CCSD(T)/6-311G(d,pd)//MP2/6-311++G** + ZPE level of theory. Because the association of $H_2O(X^1A_1)$ to $C_2(^1\Sigma_g^+)$ is exothermic by 6.4 kcal mol^{-1}, the low activation energy barrier going from **PRT2** to **I1** can be readily overcome, and the association reaction (1c) is expected to proceed rapidly. As a result, the association branch will dominate over the endothermic H-abstraction branches. This prompts us to focus on the association reaction and the subsequent reactions starting with **I1**.

For the reaction of $H_2O(X^1A_1)$ with $C_2(^1\Sigma_g^+)$, the transition state complex, T2, for reaction pathway 1c was searched at both MP2/6-311++G** and QCISD/6-311++G** levels of theory. The molecular structures calculated at these levels of theory are consistent with each other, with a difference of less than 5%. The structure of **PRT2** could not be located at the QCISD/6-311++G** level of theory due to the potential energy surface crossing. To obtain further insight into this reaction pathway, IRC calculation was performed to examine both reactants and products along the reaction path at the MP2/6-311++G** level of theory. Our IRC calculation result on reaction 1c indicates that T2 connects to **PRT2** and $CCOH_2$ as a reactant and a product, respectively, on the singlet potential surface. We tried to search for a transition state structure on the triplet potential surface but were unable to locate a saddle point that connects to triplet C_2OH_2.

Both MP2 and QCISD calculations predict very similar bond lengths for the **I1** adduct, but the CCO angle of **I1** is predicted to be 168.9° and 149.9° at the MP2 and the QCISD level, respectively. Detailed investigation of the molecular orbitals suggests that the unpaired valence electron in the internal carbon atom does not contribute to the C−O bond formation. This leads to a C−O bond length of 1.441 Å and a C−O stretch vibration frequency of 718 cm^{-1} (Table 4), which reveal a single C−O bond characteristics.

The $CCOH_2$ intermediate generated from the association process (reaction c) could be unstable due to the fact that no experimental evidence was reported of its observation. This implies that further reactions would take place following the formation of $CCOH_2$. Several reaction channels (Figure 2a) are considered in the present work for the subsequent reactions involving the $CCOH_2$ species, which are discussed in the following subsections.

Four reaction pathways leading to the formation of $H_2 + CCO$ were identified with the $CCOH_2$ as a starting reactant:

pathway 3a: **I1**-T3a-CCO + H_2

$$CCOH_2 \rightarrow [T3a]^{\ddagger} \rightarrow H_2 + CCO \quad (3a)$$

pathway 3b: **I1**-CCOH + H-T3b-CCO + H_2

$$CCOH_2 \rightarrow CCOH + H \rightarrow [T3b]^{\ddagger} \rightarrow H_2 + CCO \quad (3b)$$

pathway 3c: **I1**-T3-**I2**-T3c-**I4**-CCO + H_2

$$CCOH_2 \rightarrow [T3]^{\ddagger} \rightarrow HCCOH \rightarrow [T3c]^{\ddagger} \rightarrow H_2CCO \rightarrow H_2 + CCO \quad (3c)$$

pathway 3d:
I1-T3-**I2**-T3d1-**I3**-T3d2-c-COC + H_2-T3d3-CCO + H_2

$$CCOH_2 \rightarrow [T3]^{\ddagger} \rightarrow HCCOH \rightarrow [T3d1]^{\ddagger} \rightarrow c{-}H_2COC \rightarrow [T3d2]^{\ddagger} \rightarrow c\text{-}COC + H_2 \rightarrow [T3d3]^{\ddagger} \rightarrow H_2 + CCO \quad (3d)$$

pathway 3e: **I1**-T3-**I2**-T3d1-**I3**-T3e1-**I4**-CCO + H_2

$$CCOH_2 \rightarrow [T3]^{\ddagger} \rightarrow HCCOH \rightarrow [T3d1]^{\ddagger} \rightarrow c\text{-}H_2COC \rightarrow [T3e1]^{\ddagger} \rightarrow H_2CCO \rightarrow H_2 + CCO \quad (3e)$$

The molecular structure for each species involved in these reactions is illustrated in Figure 1. In Table 4 we find the relative energies of T3b and T3d3 based on MP2/6-311++G** are significantly different from the results of the CCSD(T)/6-311++G(d,pd)//MP2/6-311++G** level, but the structures is still more reliable than those based on QCISD/6-311++G**. The energies based on CCSD(T)/6-311++G(d,pd)//QCISD/6-311++G** are larger than those based on CCSD(T)/6-311++G(d,pd)//MP2/6-311++G** for T3b and T3d3, respectively. All transition states involved in reactions 3a−3e were checked with the IRC calculation to ensure their connection to proper reactants and products. On the basis of our calculation at the CCSD(T)/6-311G(d,pd)//MP2/6-311++G** + ZPE level of theory, the overall enthalpy of reaction 3 is −15.3 kcal mol^{-1}. Direct decomposition of $CCOH_2$ into $H_2 + CCO$ (reaction a) was found to have an activation energy barrier of 37.7 kcal mol^{-1}, whereas reactions 3b, 3c, and 3d require a minimum energy input of 25.4, 12.9, and 33.4 kcal mol^{-1}, respectively, to take place. These results suggest that a large energy barrier must be surmounted for reaction 3 to occur. Therefore, the formation of $H_2 + CCO$ from $CCOH_2$ is thermodynamically feasible but kinetically unfavorable, and reactions 3a−3e would be nearly inconceivable at low temperatures. On the basis of our computational results, the hydrogen atoms attached to the oxygen atom do not simultaneously stretch to approach each other to form a hydrogen molecule. Note that the two lowest reaction channels leading to the formation of $H_2 + CCO$ products are reactions 3b and 3c. Because reaction 3b begins with a hydrogen−oxygen bond cleavage and because H_2CCO (ketene) is the most stable species in reaction 3c, CCOH and ketene may be the feature species to be sought for experimental evidence of these reaction mechanisms.

Dissociation of $CCOH_2$ into CCOH + H is endothermic by 22.2 kcal mol^{-1}, which is higher than the activation energy of 12.9 kcal mol^{-1} for the isomerization of $CCOH_2$ into HCCOH (**I2**) via a transition state, namely, T3 (see Figure 2a). Therefore, the isomerization of $CCOH_2$ into HCCOH is expected to dominate over its H-cleavage process. We used both MP2 and QCISD levels of theory to locate the T3 for the **I1**-T3-**I2** process in reaction 3c, and both methods produced essentially identical T3 structure (see Figure 1).

3.3. Relationship between HCCOH and Various Isomer Intermediates. The energetic results calculated at the CCSD(T)/6-311G(d,pd)//MP2/6-311++G** + ZPE level of theory suggest that all reactions involving **I2**(HCCOH) as a reactant are either highly endothermic, or possess a high activation energy barrier (Figure 2b). Therefore, once HCCOH is formed, it is unlikely for this species to be isomerized into cyclic- or c-H_2-COC(**I3**), H_2CCO(**I4**), c-HCOCH(**I5**), and CCHOH(**I6**) (referred to Figure 1 for molecular structure of these species) in low-temperature interstellar environment such as diffuse clouds, transluscent clouds, and dense clouds. However, these isomers may be produced in a high-temperature environment, such as combustion flames, in one or more steps of rearrangement. For example, **I3**(c-H_2COC) can be formed through a pathway of **I2**-T3d1-**I3** with an energy barrier of 94.9 kcal mol^{-1},

$$HCCOH \rightarrow [T3d1]^{\ddagger} \rightarrow c\text{-}H_2COC \quad (3d1)$$

I4(H_2CCO) can be produced either through a pathway of **I2**-T3c1-**I4** with an energy barrier of 60.5 kcal mol^{-1},

$$HCCOH \rightarrow [T3c1]^{\ddagger} \rightarrow H_2CCO \quad (3c1)$$

or through a pathway of **I3**-T3e1-**I4** with an energy barrier of 21.3 kcal mol^{-1},

$$c\text{-}H_2COC \rightarrow [T3e1]^{\ddagger} \rightarrow H_2CCO \quad (3e1)$$

I5(c-HCOCH) can then be generated either from isomerization of **I3** via **I3**-T4-**I5** with an energy barrier of 54.9 kcal mol^{-1},

$$c\text{-}H_2COC \rightarrow [T4]^{\ddagger} \rightarrow c\text{-}HCOCH \quad (4)$$

or from isomerization of **I4** via **I4**-T5-**I5** with an energy barrier of 79.6 kcal mol^{-1},

$$H_2CCO \rightarrow [T5]^{\ddagger} \rightarrow c\text{-}HCOCH \quad (5)$$

Pathway 5 is very unfavorable, due to the low reaction barrier of the reverse reaction. So even though pathway 4 occurs, **I5**(c-HCOCH) can easily isomerize to **I4**(c-HCOCH) due to the instability of **I4** and **I6**(CCHOH) may be derived by migration of a oxygen atom over a carbon atom and insertion into a carbon−hydrogen bond in **I5**, i.e., **I5**-T6a-**I6**, with an energy barrier of 36.9 kcal mol^{-1},

$$c\text{-}HCOCH \rightarrow [T6a]^{\ddagger} \rightarrow CCHOH \quad (6a)$$

Scott et al.[33] mapped out the potential energy surface using the CCSD(T)/6-311G(p,df) level of theory for the reaction pathway of **I5** isomerization into **I4**,

$$c\text{-}HCOCH \rightarrow [TS1]^{\ddagger} \rightarrow HCC(H)O \rightarrow [TS2]^{\ddagger} \rightarrow H_2CCO \quad (6b)$$

with an activation barrier of 2 and 24 kcal mol^{-1} for the first and second transition state, respectively. Their characterization of HCC(H)O (formylmethylene) species suggests that the reaction of C_2 with water leading to formation of $CCOH_2$ and its isomers may involve at least two precomplex species, **PRT2** and HCC(H)O.

I6 can also be formed either by migration of the OH group from C2 to C1 in **I2**, i.e., **I2**-T6c-**I6**, with an energy barrier of 75.6 kcal mol^{-1},

$$HCCOH \rightarrow [T6c]^{\ddagger} \rightarrow CCHOH \qquad (6c)$$

or by migration of the hydrogen atom from C1 to C2, i.e., **I2**-T6d-**I6**, with an energy barrier of 45.8 kcal mol^{-1} below the reaction enthalpy,

$$HCCOH \rightarrow [T6d]^{\ddagger} \rightarrow CCHOH \qquad (6d)$$

Because the energy barrier for reaction 6c is higher than that of reaction 6d, hydrogen atom migration is expected to dominate over −OH group migration in the isomerization of HCCOH into CCHOH. Note that the structure of **I6** could not be located at the MP2/6-311++G** level of theory and the reverse reaction of (6d) is negative activation energy based on the QCISD/6-311++G** level, the direct consequence is that the product side of (6a)'s IRC based on MP2/6-311++G** is HCCOH. In fact, the product side of (6a)'s IRC based on QCISD/6-311++G** is HCCHOH. Species HCCOH, considered a stable configuration by QCISD/6-311++G**, is not considered a stable configuration by MP2/6-311++G**. So we located the transition state structures of T6a for reaction 6a, T6c for reaction 6c, and T6d for reaction 6d and checked them by running complete IRC at the QCISD/6-311++G** level of theory to ensure the reactant and product structures are consistent with that optimized at the MP2/6-311++G** level or QCISD/6-311++G** level. This would validate the geometry optimized at the MP2/6-311++G** level of theory for T6a and T6c, whose best estimate energetics is based on the CCSD(T)/6-311++(d,pd)//MP2/6-311++G** + ZPE level. Due to the fact that T6d and **I6** could not be located at the MP2 level, the best estimate energetics of T6d and **I6** was based on the calculation at the CCSD(T)/6-311++(d,pd)//QCISD/6-311++G** + ZPE level of theory.

Though we fail to locate T6d using MP2/6-311++G**, the detailed IRC based on QCISD/6-311++G** show a proper trend toward **I2**(HCCOH) and **I6**(CCHOH). Maybe it needs a more sophisticated quantum method and larger basis sets than currently used to define it. From the calculated results, information that **I6** is unstable can be inferred conclusively. Comparing the energy profiles of three pathways to forming **I6**(CCHOH), we suggest that even **I6** (CCHOH) formed, though T6c or T6a can easily isomerize to **I2**(HCCOH).

From the discussion, we suggest that three stable isomers are **I2**, **I3**, and **I4**, among which **I4** is the most stable isomer.

For the **I2**(HCCOH) dissociation leading to CCOH + H and HCCO + H,

$$HCCOH \rightarrow CCOH + H \qquad (7a)$$

$$HCCOH \rightarrow HCCO + H \qquad (7b)$$

a threshold energy is predicted to be 123.2 and 71.0 kcal mol^{-1} for the C−H bond and O−H bond raptures, respectively.

In addition to participation in reactions 3d, 3e1, and 4, **I3**(c-H_2COC) can also either decompose to produce CH_2 and CO through **I3**-T8a-CH_2+CO with an energy barrier of 22.3 kcal mol^{-1},

$$c\text{-}H_2COC \rightarrow [T8a]^{\ddagger} \rightarrow CH_2 + CO \qquad (8a)$$

or decompose to c-HCOC + H, which is endothermic by 96.8 kcal mol^{-1},

$$c\text{-}H_2COC \rightarrow c\text{-}HCOC + H \qquad (8b)$$

4. Astrophysical and Experimental Implications

The intermediate species and products characterized in the present study may provide some insight into interstellar and combustion chemistry. The association reaction (1c) appears to be dominant over the H-abstraction reactions on either the singlet or triplet potential energy surface, and this reaction could be the most likely step one process for the $C_2 + H_2O$ reaction in dense interstellar space (dark and cold clouds). The H-abstraction reactions could compete with the association reaction in circumstellar envelopes where abundant C_2 and H_2O exist and the temperature can be as high as 4500 K.[1] Also, the unlikely processes in diffuse, transluscent, and dense clouds, such as isomerization of **I2** into **I3**, **I4**, **I5**, and **I6**, and dissociation of these intermediates into small species, may become feasible in the circumstellar envelopes.

On the basis of our computational results we conclude that in experimentally controlled conditions **I2** can be formed as a main product through the following pathways:

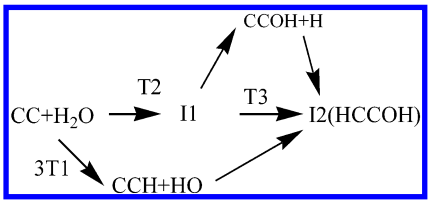

In low temperature environment of cold star clouds, only the pathway through T2-**I1**-T3-**I2** is possible.

Meanwhile, the pressure impact on the rate of forming **I2**(HCCOH) must be considered. Pathways 3a and 3b, the first intramolecular migration are the competitive reactions. Because (3a) and (3b) both form two products and pressure has on impact on intramoleuclar migration, increasing pressure is not favorable for reactions 3a and 3b and is favorable for intramolucalr migration (**I1**-T3-**I2**). So we suggest that increasing the pressure will favor the formation of **I2**(HCCOH).

The formation of stable product (**I4**, ketene) from the reaction of C_2 with water is overall the most exothermic among other processes,

$$C_2 + H_2O \rightarrow H_2CCO$$

$$\Delta_r H(298K) = -140.9 \text{ kcal mol}^{-1} \text{ (this work)}$$

$$\Delta_r H(298K) = -141.9 \text{ kcal mol}^{-1} \text{ (experiment}^{34}\text{)} \qquad (9)$$

I4 can be formed through reactions 3c1 and 3e1 at experimentally controlled high-temperature conditions. Our calculation results suggest that ketene can be a likely product from reaction 9, but there is no intermediate species that can provide the evidence for a unique reaction pathway contributing to the formation of this molecule.

5. Conclusions

In this paper, we explored the chemical dynamics of the reaction of the dicarbon molecule with water. On the singlet potential energy surface, the reaction would proceed with association of a water molecule to the dicarbon molecule through a precomplex and with a mall energy barrier, forming $CCOH_2$. Further reaction of $CCOH_2$ energetically prefers a hydrogen migration on the singlet surface to produce hydroxyacetylene (HCCOH) species. Subsequent reactions may involve further

rearrangements, leading to the formation of various isomers, among which is ketene, H_2CCO, the most stable form of the C_2OH_2 molecule. The dissociation of the C_2OH_2 isomers result in both transient and stable species as products, including H, CCOH, c-COC, H_2, c-HCOC, CCO, HCCO, CH_2, and CO. On the triplet potential surface, the reaction is characterized by H-abstraction, leading to the formation of $CCH(^2\Sigma^+)$ and $OH(^2\Sigma^+)$, which may associate to form singlet hydroxyacetylene (HCCOH).

Acknowledgment. This work is supported by NSFC (Grant Nos. 29825107, 29853001) and NKBRSF.

Supporting Information Available: Table of total energies, zero point energies, relative energies, and moments of inertia. This material is available free of charge via the Internet at http://pubs.acs.org.

References and Notes

(1) Kaiser, R. I. *Chem. Rev.* **2002**, *102*, 1309.
(2) Gaydon, A. G.; Wolfhard, H. G.; Fames, Chapman & Hall: New York, 1979.
(3) Perry, M. D.; Raff, L. M. *J. Phys. Chem*. **1994**, *98*, 4375.
(4) O'Brien, S. C.; Heath, J. R.; Curl, R. F.; Smalley, R. E. *J. Chem. Phys*. **1988**, *88*, 220.
(5) Weltner, J. W.; Van Zee, R. *Chem. Rev.* **1989**, *89*, 1713.
(6) Balucani, N.; Mebel, M. A.; Lee, Y. T.; Kaiser, R. I. *J. Phys. Chem. A* **2001**, *105*, 9814.
(7) Kaiser, R. I.; Le, T. N.; Nguyen, T. L.; Mebel, A. M.; Balucani, N.; Lee, Y. T.; Stahi, F. *Faraday Discuss.* **2001**, *119*, 51.
(8) Ding, Y. H.; Li, Z. S.; Huang, X. R.; Sun, C. C. *J. Chem. Phys*. **2000**, *113*, 1745.
(9) Zhang, X.; Ding, Y. H.; Li, Z. S.; Huang, X.-R.; Sun, C. C. *Chem. Phys. Lett*. **2000**, *330*, 577.
(10) Kruse, T.; Roth, P. J. *Chem. Phys. Lett*. **1997**, *101*, 2138.
(11) Kaiser, R. I.; Yamada, M.; Osamura, Y. *J. Phys. Chem*. **2002**, *106*, 4825.
(12) Cenicharo, J.; Conzalez-Alfonso, I.; Lefloch, B. *ESA SP-419* **1997**, 23.
(13) Ehrenfreund, P.; Boogert, A. C. A.; Gerakines, P. A.; Schutte, W. A.; Thi, W. F.; Tielens, A. G. G. M.; Vandenbussche, B.; Van Dishoeck, E. F.; Whittet, D. C. B. *ESA SP-419* **1997**, 3.
(14) Melnick, G. J.; Dalgarno, A.; Erickson, N. R.; Fazio, G. G.; Goldsmith, P. F.; Harwit, M.; Hollenbach, D. J.; Koch, D. G.; Neufeld, D. A.; Schieder, R.; Snell, R. L.; Stauffer, J. R.; Thaddeus, P.; Tolls, V.; Winnewisser, G. F. *ESA SP-401* **1997**, 189.
(15) Spaans, M.; Van Dishoeck, E. F. *Astrophys. J*. **2001**, *548*, L217.
(16) De Muizon, M. J.; Ehrenfreund, P.; Dartois, E.; Habing, H. J.; Puget, J. L.; Breitfellner, M. *Adv. Space Res*. **1998**, *21*, 11.
(17) Frisch, M. J.; Trucks, G. W.; Schlegel, H. B.; Scuseria, G. E.; Robb, M. A.; Cheeseman, J. R.; Zakrzewski, V. G.; Montgomery, J. A., Jr.; Stratmann, R. E.; Burant, J. C.; Dapprich, S.; Millam, J. M.; Daniels, A. D.; Kudin, K. N.; Strain, M. C.; Farkas, O.; Tomasi, J.; Barone, V.; Cossi, M.; Cammi, R.; Mennucci, B.; Pomelli, C.; Adamo, C.; Clifford, S.; Ochterski, J.; Petersson, G. A.; Ayala, P. Y.; Cui, Q.; Morokuma, K.; Malick, D. K.; Rabuck, A. D.; Raghavachari, K.; Foresman, J. B.; Cioslowski, J.; Ortiz, J. V.; Stefanov, B. B.; Liu, G.; Liashenko, A.; Piskorz, P.; Komaromi, I.; Gomperts, R.; Martin, R. L.; Fox, D. J.; Keith, T.; Al-Laham, M. A.; Peng, C. Y.; Nanayakkara, A.; Gonzalez, C.; Challacombe, M.; Gill, P. M. W.; Johnson, B.; Chen, W.; Wong, M. W.; Andres, J. L.; Gonzalez, C.; Head-Gordon, M.; Replogle, E. S.; Pople, J. A. *Gaussian98*, revision X.X; Gaussian, Inc.: Pittsburgh, PA, 1998.
(18) Moller, C.; Plesset, M. S. *Phys. Rev.* **1934**, *46*, 618.
(19) Head-Gordon, M.; Pople, J. A.; Frisch, M. J. *Chem. Phys. Lett.* **1988**, *153*, 503.
(20) Frisch, M. J.; Head-Gordon, M.; Pople, J. A. *Chem. Phys. Lett*. **1990**, *166*, 275.
(21) Frisch, M. J.; Head-Gordon, M.; Pople, J. A. *Chem. Phys. Lett*. **1990**, *166*, 281.
(22) Head-Gordon, M.; Head-Gordon, T. Analytic MP2 Frequencies Without Fifth Order Storage: Theory and Application to Bifurcated Hydrogen Bonds in the Water Hexamer. *Chem. Phys. Lett*. **1994**, *220*, 122.
(23) Trucks, G. W.; Frisch, M. J.; Andres, J. L.; Schlegel, H. B. An Efficient Theory and Implementation of MP2 Second Derivatives. **1998**.
(24) Saebo, S.; Almlof, J. *Chem. Phys. Lett.* **1989**, *154*, 83.
(25) (a) Frisch, M. J.; Pople, J. A.; Binkley, J. S. *J. Chem. Phys.* **1984**, *80*, 3265. (b) Clark, J.; Chandrasekhar, T.; Spitznagel, G. W.; Schleyer, P. v. R. *J. Comput. Chem.* **1983**, *4*, 294. (c) Frisch, M. J.; Pople, J. A.; Binkley, J. S. Self-Consistent Molecular Orbital Methods 25: Supplementary Functions for Gaussian Basis Sets. *J. Chem. Phys.* **1984**, *80*, 3265.
(26) Pople, J. A.; Head-Gordon, M.; Raghavachari, K. *J. Chem. Phys*. **1987**, *87*, 5968.
(27) Gauss, J.; Cremer, C. *Chem. Phys. lett*. **1988**, *150*, 280.
(28) (a) Fukui, K. *J. Phys. Chem*. **1970**, *74*, 4161. (b) Gonzalez, C.; Schlegel, H. B. *J. Phys. Chem*. **1990**, *94*, 5523. (c) Gonzalez, C.; Schlegel, H. B. *J. Chem. Phys.* **1989**, *90*, 2154.
(29) (a) Ishida, K.; Morokuma, K.; Komornicki, A. *J. Chem. Phys.* **1977**, *66*, 2153. (b) Muller, K. *Angew. Chem., Int. Ed. Engl.* **1980**, *19*, 1. (c) Schmidt, M. W.; Gordon, M. S.; Dupuis, M. *J. Am. Chem. Soc.* **1985**, *107*, 2585. (d) Garrett, B. C.; Redmon, M. J.; Steckler, R.; Truhlar, D. G.; Baldridge, K. K.; Bartol, D.; Schmidt, M. W.; Gordon, M. S. *J. Phys. Chem.* **1988**, *92*, 1476. (e) Baldridge, K. K.; Gordon, M. S.; Steckler, R.; Truhlar, D. G. *J. Phys. Chem.* **1989**, *93*, 5107. (f) Gonzales, C.; Schlegel, H. B. *J. Chem. Phys.* **1989**, *90*, 2154.
(30) Purvis, G. D.; Bartlett, R. J. *J. Chem. Phys.* **1982**, *76*, 1910.
(31) Raghavachari, K.; Trucks, G. W.; Pople, J. A.; Head-Gordon, M. *Chem. Phys. Lett.* **1989**, *157*, 479.
(32) Reisler, H.; Mangir, M.; Witting, C. *J. Chem. Phys.* **1979**, *71*, 2109.
(33) Scott, A. P.; Nobes, R. H.; Schaefer, H. F.; Radom, L. *J. Am. Chem. Soc*. **1994**, *116*, 101599.
(34) Donald, D. W.; Willam, H. E.; Vivian, B. P.; Richard, H. S.; Iva, H.; Sylvia, M. B.; Kenneth, L. C.; Ralph, L. N. *NBS Tables of Chemical Thermodynamics*; NBS: Washington, DC, 1998.